Mechanical stimulations can inhibit local and remote tumor progression by downregulating WISP1

Shengzhi Liu[1], Di Wu[1,2], Xun Sun[1,2], Yao Fan[1,2], Rongrong Zha[1,2], Aydin Jalali[1], Meghana Teli[1], Tomonori Sano[1,3], Amanda Siegel[4,5], Akihiro Sudo[3], Mangilal Agarwal[4,6], Alexander Robling[7,8], Bai-Yan Li[2], and Hiroki Yokota[1,2,4,6,7,8,9*]

[1]Department of Biomedical Engineering, Indiana University Purdue University Indianapolis, Indianapolis, IN 46202, USA
[2]Department of Pharmacology, School of Pharmacy, Harbin Medical University, Harbin 150081, China
[3]Department of Orthopedic Surgery, Mie University, Mie 514, Japan
[4]Integrated Nanosystems Development Institute, Indiana University Purdue University Indianapolis, Indianapolis, IN 46202, USA
[5]Department of Chemistry and Chemical Biology, Indiana University Purdue University Indianapolis, Indianapolis, IN 46202, USA
[6]Department of Mechanical Engineering, Indiana University Purdue University Indianapolis, Indianapolis, IN 46202, USA
[7]Department of Anatomy and Cell Biology, Indiana University School of Medicine, Indianapolis, IN 46202, USA
[8]Indiana Center for Musculoskeletal Health, Indiana University School of Medicine, Indianapolis, IN 46202, USA
[9]Simon Cancer Center, Indiana University School of Medicine, Indianapolis, IN 46202, USA

Running Title: Mechanical loading and tumor suppression
Key Words: breast cancer, bone metastasis, urine, cholesterol, TGFβ, calcitriol, vitamin D_3, WISP1

* Corresponding author

This is the author's manuscript of the article published in final edited form as:

Liu, S., Wu, D., Sun, X., Fan, Y., Zha, R., Jalali, A., Teli, M., Sano, T., Siegel, A., Sudo, A., Agarwal, M., Robling, A., Li, B.-Y., & Yokota, H. (2020). Mechanical stimulations can inhibit local and remote tumor progression by downregulating WISP1. FASEB Journal: Official Publication of the Federation of American Societies for Experimental Biology, 34(9), 12847–12859. https://doi.org/10.1096/fj.202000713RR

Nonstandard Abbreviations

Ang2: angiopoietin 2; ANOVA: analysis of variance; BMD: bone mineral density; bpm: beats per minute; BV/TV: bone volume density; CN: control; CO2: carbon dioxide; DMEM: Dulbecco's modified eagle medium; EdU: 5-ethynyl-2′-deoxyuridine; ELISA: enzyme-linked immunosorbent assay; FDA: Food and Drug Administration; FKN: fractalkine; GEPIA: gene expression profiling interactive analysis; GTEx: Genotype Tissue Expression; H&E: Haematoxylin and Eosin; Hz: hertz; MMP9: matrix metallopeptidase 9; mRNA: messenger RNA; NFATc1: nuclear factor of activated T cells 1; PAP3: purple acid phosphatase 3; PBS: phosphate-buffered saline; PCA: principal component axis; Tb.n: trabecular number; and Tb.s: trabecular separation.

Abstract

Mechanical stimulations can prevent bone loss, but their effects on the tumor-invaded bone or solid tumors are elusive. Here, we evaluated the effect of knee loading, dynamic loads applied to the knee, on metastasized bone and mammary tumors. In a mouse model, tumor cells were inoculated to the mammary fat pad or the proximal tibia. Daily knee loading was then applied and metabolic changes were monitored mainly through urine. Urine samples were also collected from human subjects before and after step aerobics. The result showed that knee loading inhibited tumor progression in the loaded tibia. Notably, it also reduced remotely the growth of mammary tumors. In the urine, an altered level of cholesterol was observed with an increase in calcitriol, which is synthesized from a cholesterol derivative. In urinary proteins, knee loading in mice and step aerobics in humans markedly reduced WNT1-inducible signaling pathway protein 1, WISP1, which leads to poor survival among patients with breast cancer. In the *ex vivo* breast cancer tissue assay, WISP1 promoted the growth of cancer fragments and upregulated tumor-promoting genes such as Runx2, MMP9, and Snail. Collectively, the present preclinical and human study demonstrated that mechanical stimulations such as knee loading and step aerobics altered urinary metabolism and downregulated WISP1. The study supports the benefit of mechanical stimulations for locally and remotely suppressing tumor progression. It also indicated the role of WISP1 downregulation as a potential mechanism of loading-driven tumor suppression.

Introduction

Physical activity is considered to modulate the levels of hormones, prevent obesity, improve immune system functions, and alter the metabolism (1). Epidemiologic studies indicate that physical activity reduces the risk of cancer induction in the colon, endometrium, breast, and others (2). While weight-bearing physical activity and skeletal loading are known to enhance bone formation (3, 4), little is known about the role of loading-driven regulation of tumor-invaded bone or non-skeletal solid tumors. Here, we examined the effects of skeletal loading on the knee on the progression of tumors. Since bone is a frequent metastasis site from advanced breast cancer (5), we evaluated loading effects on the mammary tumor and tumor-invaded tibia.

Knee loading is one form of joint loading modalities, in which oscillatory, compressive loads are applied to a synovial joint such as the knee, ankle, and elbow (6). In pre-clinical studies using a mouse model, we and others have shown that knee loading can enhance bone formation (7), accelerate the healing of necrotic femoral head (8), and reduce inflammation in the arthritic knee (9). It is also reported that knee loading can activate neuronal signaling and elevate the serotonin level in the brain (10). We have previously shown that ankle loading, the other form of joint loading modality, ameliorated tumor-driven bone loss by inhibiting the nuclear factor of activated T-cells cytoplasmic 1 (NFATc1)-driven bone resorption in the loaded tibia (11). However, little is known about loading effects on systemic metabolites or tumorigenesis that is not directly linked to bone homeostasis. Loading-linked therapy is important in many diseases including cancers since it generally does not induce life-threatening side effects and it is cost-effective as a combined regimen with other treatments. The question herein is whether knee loading can inhibit the progression of primary and metastasized tumors at the loaded and non-

loaded sites by regulating tumor-promoting and suppressing metabolites and genes.

To evaluate local and global changes in metabolism, we analyzed urinary metabolites since urine can be collected in a large volume relatively with ease. In our previous study with Pitavastatin (12), which is an FDA-approved drug to lower the cholesterol level (13), we showed that Pitavastatin altered urinary metabolites in the mevalonate pathway in a mouse model of breast cancer. We have also shown that axial tibia loading in a mouse model or step aerobics in human subjects can sharply reduce the level of cholesterol and elevate the levels of dopamine, and melatonin in urine, in which dopamine and melatonin serve as tumor-suppressing agents (14). Although mechanical stimulations were shown to convert the urine into an anti-tumor agent, the mechanical effects with knee loading on the growth of mammary tumors and loaded tumor-invaded bones have not been elucidated.

In this study, we focused on three biomarkers in the urine: cholesterol as a potential tumor-promoting agent (15), TGFβ as a growth factor to induce a bone-resorbing vicious cycle (16), and 1,25-dihydroxy vitamin D_3 (calcitriol) as a potential tumor-suppressing agent (17). Interestingly, vitamin D_3 is synthesized in the skin from 7-dehydrocholesterol, a derivative of cholesterol (18). We chose these biomarkers since they are considered to be involved in tumor progression and bone metabolism. We examined whether a dynamic urinary balance of cholesterol, TGFβ, and calcitriol would be altered by knee loading. We also conducted antibody array analysis and identified Wnt1 inducible signaling pathway protein 1, WISP1, a proto-oncogene protein in a member of CCN family (19), as a critical regulator in the responses to cholesterol, TGFβ, and calcitriol. Calcitriol is known to be an inhibitor of WISP1 (20), and

WISP1 is reported to promote tumor growth by attenuating p53-mediated apoptosis (21). To further evaluate the outcome with the mouse model, human urine samples were examined before and after weight-bearing physical activity (step aerobics). The cancer genome atlas (TCGA) and Genotype Tissue Expression (GTEx) databases were also used to assess the clinical significance of WISP1 in cancer tissues.

Materials and Methods

Cell culture

EO771 mouse mammary tumor cells (CH3 BioSystems, Amherst, NY, USA) (22) were cultured in DMEM with 10% fetal bovine serum and antibiotics, and cells were maintained at 37°C and 5% CO_2. Cellular proliferation was examined using a fluorescence-based cell proliferation kit (Click-iT™ EdU Alexa Fluor™ 488 Imaging Kit; Thermo-Fisher, Waltham, MA, USA) as previously described (23). A Transwell chamber assay was conducted to detect invasive cellular motility (24), and a wound-healing scratch assay was utilized to evaluate 2-dimensional migratory behavior (25).

Western blot analysis and protein array analysis

Western blot analysis was conducted using the procedure previously described (26). A luminescent image analyzer (LAS-3000, Fuji Film, Tokyo, Japan) was used to capture signals and ImageJ (NIH, Bethesda, MD, USA) was used to quantify signal levels. We used antibodies against Runx2 (8486s), Snail (3879s), TGFβ (3711s) (Cell Signaling, Danvers, MA, USA), WISP1 (AF1689, R&D Systems, Minneapolis, MN, USA), MMP9 (sc-393859) (Santa Cruz, Dallas, TX, USA), and β-actin (A5441, Sigma, Saint Louis, MO, USA). We also employed a mouse XL cytokine array (R&D Systems, Minneapolis, MN, USA) and determined expression of 111 cytokines and chemokines in mouse urine samples.

Animal models

The experimental procedures were approved by the Indiana University Animal Care and Use Committee and complied with the Guiding Principles in the Care and Use of Animals endorsed

by the American Physiological Society. Mice were housed five per cage in a pathogen-free condition and provided with mouse chow and water *ad libitum*. In the mouse model of the mammary tumor, mice were randomly assigned into two groups (placebo and knee loading). Eight-week-old C57BL/6 female mice (8 per group; Envigo RMS, Inc., Indianapolis, IN, USA) received subcutaneous injections of EO771 cells (3.0×10^5 cells in 50 μl PBS), to the mammary fat pad on day 0 (25). In the mouse model of tibial osteolysis, C57BL/6 female mice (8 per group) were randomly assigned into two groups (placebo and knee loading) and they received the injection of EO771 cells (3.0×10^5 cells in 20 μl PBS) to the right tibia. On day 14 the animals were sacrificed 30 min after the last knee loading, and urine and serum samples were collected from the healthy control (12 mice), placebo (8 mice), and knee loading groups (8 mice) (Fig. 1A).

Knee loading and strain measurement

To the knee loading group, knee loading was applied daily using an ElectroForce device (TA Instruments, New Castle, DE, USA) from day 1 after tumor inoculation on day 0. Mice were anesthetized with ~1.5% isoflurane, and sinusoidal loads of 0.5 N (peak-to-peak) at 2 Hz were given to the left knee for 5 min. Mice in the placebo group were anesthetized and placed on the loading device without receiving dynamic loads. No adverse effects in response to knee loading were observed.

Strain in response to knee loading was measured using a strain measurement unit (EDX-14A; Kyowa Americas Inc., Novi, MI, USA). A pair of strain gauges (SKF-27085, 200 μm gauge

length; Kyowa America Inc.) was immobilized to the proximal tibia in an orthogonal direction, and the tibia was compressed with 0.5, 1, or 2 N loads at 1 Hz.

μCT imaging and histology

The tibiae were harvested for μCT imaging and histology, and the samples were blinded for further analysis. Micro-CT was performed using Skyscan 1172 (Bruker-MicroCT, Kontich, Belgium). Using manufacturer-provided software, scans were performed at pixel size 8.99 μm and the images were reconstructed (nRecon v1.6.9.18) and analyzed (CTan v1.13). In histology, H&E staining was conducted as described previously (25).

Volatile organic compounds (VOCs) and ELISA

Six to seven urine samples in the placebo and knee loading groups and twelve samples in the control group were collected from mice before and 30 min after knee loading. VOCs were identified using solid-phase micro-extraction, coupled to a 7200 Accurate Mass Quadruple Time of Flight mass spectrometer (Agilent Technologies, Santa Clara, CA, USA) (26). Data were analyzed using MassHunter Quantitative Profinder software (B.08.00; Agilent Technologies). Relative abundances were calculated and $\log_2$ transformed-16, and hierarchical clustering analysis and principal component analysis were conducted. Using ELISA kits, the levels of TGFβ (Thermo Fisher), cholesterol (MyBioSource, San Diego, CA, USA), and calcitriol (1,25-dihydroxy vitamin D_3) (AVIVA Systems Bio, San Diego, CA, USA) in the serum and urine were determined.

Ex vivo breast cancer tissue assay

The usage of human breast cancer tissues was approved by the Indiana University Institutional Review Board. A sample (~ 1 g; ER/PR+, HER2+), received from Simon Cancer Center Tissue Procurement Core, was manually fragmented with a scalpel into small pieces (~ 1 mm in length). These pieces were grown in DMEM with 10% fetal bovine serum and antibiotics for a day. WISP1 recombinant protein or calcitriol was then added for two additional days, and a change in the fragment size was determined.

Human urine collection

Human urine collection was approved by the Indiana University Institutional Review Board. We obtained urine samples from 10 healthy participants (5 male and 5 female; average age, 28 ± 7 years). Human subjects conducted 30-min weight-bearing physical activity, which included 10-min warming up at 80 beats per minute (bpm), 10-min core step aerobics at 120 bpm, and 10-min cooling down at 80 bpm. Urine was collected before and 1 h after physical activity.

Gene expression profiling interactive analysis (GEPIA)

Using a GEPIA server (27) for accessing TCGA (The Cancer Genome Atlas) and GTEx (Genotype-Tissue Expression) databases, the survival rate was obtained for breast cancer patients with high and low levels of WISP1. The correlation coefficients for mRNA levels in musculoskeletal tissues and breast cancer tissues were determined. Data are given on a logarithmic scale (base 2) with a unit of transcript per million (TPM).

Statistical analysis

For cell-based experiments, three or four independent experiments were conducted and data were expressed as mean ± S.D. In animal experiments, the sample size in the mouse model was chosen to achieve a power of 80% with $p < 0.05$. The primary experimental outcome was tumor weight for the mammary fat pad experiment and the bone volume ratio (BV/TV) for the tibia experiment. The secondary experimental outcome was tumor size for the mammary fat pad experiment and the trabecular number (Tb.n) for the tibia experiment. All data were tested for normality (Shapiro–Wilk normality test) and statistical significance was evaluated using a one-way analysis of variance (ANOVA). Post hoc statistical comparisons with control groups were performed using Bonferroni correction with statistical significance at $p < 0.05$. The single and double asterisks in the figures indicate $p < 0.05$ and $p < 0.01$, respectively.

Results

Knee loading suppressed tumor progression in the tumor-invaded tibia.

As a mouse model of skeletal loading with C57BL/6 female mice, we conducted knee loading that applied sinusoidal compressive loads to the knee (Suppl. Fig. 1A). Dynamic loads of 0.5, 1, and 2 N at 2 Hz induced loading magnitude-dependent strain. Loads of 0.5 N (peak-to-peak), which will be used hereafter, induced approximately 100 με (axial compression) and 50 με (lateral tension), with a phase shift of ~180° between these two strains (Suppl. Fig. 1B).

We first examined local loading effects. EO771 mammary tumor cells were inoculated to the tibia, and daily knee loading (0.5 N loads at 2 Hz) was applied for 5 min/bout for 2 weeks (Fig. 1A). μCT images revealed that knee loading significantly reduced tumor-driven osteolysis in the proximal tibia (Fig. 1B). Compared to the placebo group, the loaded group showed well-preserved trabecular bone with an increase in BV/TV ($p = 0.0052$), BMD ($p = 0.0067$), and Tb.n ($p = 0.0057$), as well as a decrease in Tb.s ($p = 0.0401$) (Fig. 1C). While a majority of tumor cells were kept in the tibia, the femur also received tumor invasion. Compared to the placebo group, knee loading elevated BV/TV ($p = 0.0261$), BMD ($p = 0.0403$), and Tb.n ($p = 0.0427$) in the distal femur (Fig. 1D&E). H&E-stained histological images showed that compared to the placebo group, the loaded group markedly reduced the tumor-invaded area in the proximal tibia (Fig. 1F). Knee loading also downregulated TGFβ, Runx2, MMP9, and Snail in bone marrow-derived cells in the tibia (Fig. 1G).

Knee loading remotely reduced tumor growth in the mammary fat pad.

We next examined the remote loading effect on tumor growth in the mammary fat pad (Fig. 2A). Interestingly, daily knee loading significantly reduced the weight and size of the mammary tumor (p = 0.0267 and 0.0006, respectively, Fig. 2B-D). Thus, knee loading presented both local and remote loading effects.

Knee loading altered volatile organic compounds (VOCs).

The effect of knee loading was evident not only at the local site in the hind limb but also at the remote site in the upper body. To detect any systemic changes in metabolism, we first focused on urine-derived VOCs. Using 22 VOCs that presented statistical significance among any pair of 3 groups (control, placebo control, and knee loaded), hierarchical clustering analysis was conducted (Fig. 3A). In the principal component analysis, 2 clusters of VOCs were identified along the first principal component axis, in which the right cluster corresponded to the tumor-enriched VOCs (Fig. 3B). Among the tumor-enriched compounds, 5 VOCs (alpha/beta-famesene, linalool, isoprenyl alcohol, and beta-pinene) were linked to the mevalonate pathway that leads to cholesterol synthesis (Fig. 3C&D). An ELISA assay showed that compared to the control group the urinary levels of cholesterol were elevated in the placebo group, while compared to the placebo group the urinary and serum levels were lowered in the loaded group (Fig. 4A). Collectively, VOCs and ELISA data indicate that knee loading induces not only local changes in gene expression but also global metabolic alterations.

Cholesterol stimulated proliferation and invasion of tumor cells.

Although no significant difference was observed in the serum between the control and placebo groups, the urinary cholesterol level was elevated in the placebo group (Fig. 4A). We thus

evaluated the action of cholesterol on mammary tumor cells. In response to 10 μM cholesterol, the EdU-based proliferation of EO771 cells was elevated (Suppl. Fig. 2A) and cellular invasion and migration were also promoted (Suppl. Fig. 2B&C). Furthermore, the protein levels of tumor-promoting genes such as TGFβ, Runx2, MMP9, and Snail were upregulated in a dose-dependent fashion (Suppl. Fig. 2D).

Loading induced alterations in TGFβ and calcitriol.

Besides the loading-driven change in cholesterol, knee loading altered the level of TGFβ in the serum and urine (Fig. 4B). Similar to the response to cholesterol, treatment of EO771 cells with TGFβ elevated Runx2, MMP9, and Snail (Fig. 4C). In contrast, compared to the samples collected before knee loading, knee loading elevated calcitriol in the serum and urine (Fig. 4D), and calcitriol reduced Runx2, MMP9, and Snail in EO771 cells (Fig. 4E). Furthermore, calcitriol acted as a tumor suppressor by inhibiting proliferation, invasion, and migration of EO771 cells (Fig. 4F-H).

Knee loading decreased WISP1 in murine urine.

The result so far revealed that knee loading significantly affected the levels of tumor-promoting cholesterol and TGFβ, while it elevated tumor-suppressing calcitriol. These results indicated the possibility of differentially expressed oncogenes in the urine samples with and without knee loading. To detect the potential difference, we conducted antibody array analysis using a pair of pre- and post-loading urine samples. Among 111 cytokines and chemokines in the array, we observed 5 candidate genes, such angiopoietin 2 (Ang2), WISP1, fractalkine (FKN), purple acid phosphatase 3 (PAP3), and transferrin (TF), whose protein levels were reduced in the post-

loading urine sample (Fig. 5A). In TCGA and GTEx transcript databases, 4 candidates (Ang2, FKN, PAP3, and TF) except for WISP1 did not show any increase in their transcript levels in breast cancer tissues nor a significant impact on the overall survival rate (Suppl. Fig. S3). Hereafter, we focused on WISP1 that was linked to loading-sensitive Wnt signaling and known to promote tumor growth.

In response to WISP1, we observed that the proliferation of EO771 cells was elevated (Fig. 5B). WISP1 also increased the Transwell-based invasion and scratch-driven migration of EO771 cells (Fig. 5C&D). Furthermore, TGFβ, Snail, MMP9, and Runx2 were increased by WISP1 (Fig. 5E). Also, we observed that knee loading downregulated WISP1 in bone marrow-derived cells in the tibia (Suppl. Fig. S4A). Furthermore, WISP1 was elevated by cholesterol and TGFβ, while it was suppressed by calcitriol (Suppl. Fig. S4B-D). In the *ex vivo* breast cancer tissue assay, WISP1 enlarged the fragmented cancer tissues, while calcitriol reduced their size (Fig. 5F).

Loading-conditioned urine reduced WISP1, MMP9, Runx2, and TGFβ.

To evaluate the effect of loading-driven downregulation of WISP1 in urine, we grew EO771 cells in the presence of 2% urine in the culture medium. Notably, incubation with each of 10 human urine samples after post-step aerobics reduced the level of WISP1, MMP9, Runx2, and TGFβ (Fig. 6A&B; Suppl. Fig. S5A). Furthermore, incubation with each of 10 murine urine samples after knee loading reduced the protein levels of these tumor-promoting genes (Fig. 6C&D; Suppl. Fig. S5B).

High WISP1 expression was linked to the poor prognosis of breast cancer.

We have shown so far that WISP1 is one of the critical effectors in response to skeletal loading. Knee loading counteracted to the cancer-driven increase in TGFβ and WISP1 in the urine, while it elevated calcitriol in the serum and urine. TCGA and GTEx transcript databases revealed that the level of WISP1 was elevated in patients with breast cancer (Fig. 7A), and among the patients, a high level of WISP1 led to a significant reduction in the overall survival (Fig. 7B). Correlational analysis among WISP1, TGFβ, Runx2, and Snail transcripts revealed that their expression levels are positively correlated in skeletal tissues (Fig. 7C) and breast cancer tissues (Fig. 7D).

Discussion

We presented that knee loading suppressed tumor progression locally in the proximal tibia and remotely in the mammary fat pad. In the mouse urine and serum, tumor-promoting factors such as cholesterol and TGFβ were significantly altered in the loaded group. Furthermore, compared to the sham-loaded placebo group a tumor-suppressing factor, calcitriol, was increased in the loaded group in the serum and urine. The urinary changes *in vivo* were consistent with the *in vitro* evaluation. Cholesterol stimulated the proliferation of tumor cells and elevated the protein levels of tumor-promoting genes such as Runx2 (28), MMP9 (29), Snail (30), and TGFβ in EO771 mammary tumor cells, while calcitriol presented the opposite effects. Notably, the urinary level of WISP1, which lowered the overall survival rate of patients with breast cancer, was decreased in the urine after mechanical stimulations (Fig. 7E). Collectively, mechanical stimulations presented local and global anti-tumor effects in the mouse model of breast cancer, and step aerobics by human subjects supported the loading-driven regulation of WISP1 in urinary metabolism. Of note, in our previous study mechanical stimulation was shown to downregulate CSF1, macrophage colony-stimulating factor, and CD105, a tumor-promoting glycoprotein in the urine (14).

The present study demonstrated that daily loading for 5 min (600 bouts per day) prevented tumor progression not only at the loaded site but also at a remote site at the mammary fat pad. The beneficial loading effect was accompanied by the downregulation of Runx2, MMP9, and Snail in the bone marrow of the loaded tibia, as well as the metabolic VOC changes in the mevalonate pathway for cholesterol synthesis. Vitamin D_3 is synthesized from a derivative of cholesterol in the skin. Knee loading served as a metabolic switch for altering a dynamic balance from

cholesterol as a tumor promoter to calcitriol as a tumor suppressor. Of note, we focused in this study on the active form of vitamin D_3, 1,25-dihydroxyvitamin D_3, known as calcitriol that is approved for medical use for the treatment of hypocalcaemia, chronic kidney disease, and osteoporosis (31).

WISP1 regulates cellular proliferation, migration, and adhesion to the extracellular matrix and it is reported to promote tumor growth by inhibiting p53-driven apoptosis (21). Using TCGA and GTEx databases, we showed that WISP1 was highly expressed in patients with breast cancer and high WISP1 expression correlated with a poor overall survival rate. The result herein also showed that WISP1 was elevated by cholesterol and reduced by calcitriol. Furthermore, WISP1 was an inducer of TGFβ, Snail, MMP9, and Runx2 in mammary tumor cells. Taken together, the present study indicated that WISP1 was a mechano-sensitive regulator and its loading-driven downregulation suppressed tumor progression in the mammary fat pad and the tibia.

Besides the biomarkers in the serum, we also analyzed metabolic responses in mouse urine. The beneficial effect of knee loading was tracked to systemic changes in metabolites. The principal component analysis revealed that the tumor samples enriched several metabolites in the mevalonate pathway in urine-derived VOCs, while knee loading exerted the opposite effect. Consistent with the changes in VOCs, the level of cholesterol was elevated in the urine and serum. The result herein is in agreement with the potential involvement of cholesterol in tumor progression. Further analysis is needed to examine the possibility of using VOCs to evaluate the efficacy of therapeutic interventions.

This work demonstrates the active role of skeletal loading in WISP1 inhibition via cholesterol downregulation and calcitriol upregulation. While the results herein reveal a novel possibility of knee loading as adjuvant physical therapy, the study has a few limitations. C57BL/6 mouse strain was used because of its responsiveness to mechanical loading. We also employed the triple-negative mammary tumors, which are difficult to treat, and the estrogen receptor-positive breast cancer tissue, which frequently metastasizes to bone. The response to knee loading may depend on cancer types, including the hormone-receptor status since mechanical loading may affect hormonal regulation. The loading conditions are largely different in pre-clinical studies and clinical applications. As a knee loading apparatus for human use, the application of FDA-approved continuous passive motion devices after knee surgery can be considered (32). These devices are used for rehabilitation to enhance joint mobility. Besides loading to the skeletal system, weight-bearing physical activity induces varying responses in the cardiovascular system, immune system, and neurological systems (33, 34), and other systems may also be involved in the observed dynamic shift in cholesterol and calcitriol in the urine. In human urine analysis, potential bias may include the age and health conditions of individual participants and it is possible that the alterations in the selected biomarkers in the urine may not completely represent those in the primary and metastasized tumors.

In summary, this study revealed that mechanial loading suppresses local and systemic tumor progression, which was associated with an altered balance of cholesterol and calcitriol, as well as the regulation of TGFβ and WISP1. It is for the first time shown that calcitriol and WISP1 are involved in the responses to knee loading. WISP1 is exceedingly expressed in tumor tissues, and its high transcript level markedly lowers the overall survival rate of patients with breast cancer.

Collectively, the results suggest that physical activity can serve as an adjuvant cancer therapy, and the urine may serve as a diagnostic indicator in response to physical activities.

Acknowledgments

This study was in part supported by the funds from a breast cancer advocacy group, 100 Voices of Hope, as well as NIH R01AR52144, R03CA238555 (HY) and R01AR053237 (AGR).
The authors appreciate Chuanpeng Dong and Yunlong Liu for bioinformatics analysis. The authors made no disclosures.

Author Contributions

S. Liu, A. Siegel, A. Sudo, M. Agarwal, A. Robling, B. Li, and H. Yokota designed the study; S. Liu, D. Wu, X. Sun, Y. Fan, R. Zha, A. Jalali, M. Teli, and T. Sano collected and interpreted data; S. Liu, A. Robling, and H. Yokota drafted the manuscript; and all authors reviewed the manuscript and approved the final draft.

References

1. de Boer, M. C., Worner, E. A., Verlaan, D., and van Leeuwen, P. A. M. (2017) The Mechanisms and Effects of Physical Activity on Breast Cancer. *Clin Breast Cancer* **17**, 272-278
2. Friedenreich, C. M., Shaw, E., Neilson, H. K., and Brenner, D. R. (2017) Epidemiology and biology of physical activity and cancer recurrence. *J Mol Med (Berl)* **95**, 1029-1041
3. McNeely, M. L., Campbell, K. L., Rowe, B. H., Klassen, T. P., Mackey, J. R., and Courneya, K. S. (2006) Effects of exercise on breast cancer patients and survivors: a systematic review and meta-analysis. *CMAJ* **175**, 34-41
4. Coughlin, S. S., Caplan, L., Stone, R., and Stewart, J. (2019) A review of home-based physical activity interventions for breast cancer survivors. *Curr Cancer Rep* **1**, 6-12
5. Salvador, F., Llorente, A., and Gomis, R. R. (2019) From latency to overt bone metastasis in breast cancer: potential for treatment and prevention. *J Pathol* **249**, 6-18
6. Zhang, P., Malacinski, G. M., and Yokota, H. (2008) Joint loading modality: its application to bone formation and fracture healing. *Br J Sports Med* **42**, 556-560
7. Zhang, P., Tanaka, S. M., Jiang, H., Su, M., and Yokota, H. (2006) Diaphyseal bone formation in murine tibiae in response to knee loading. *J Appl Physiol (1985)* **100**, 1452-1459
8. Zhang, P., and Yokota, H. (2011) Knee loading stimulates healing of mouse bone wounds in a femur neck. *Bone* **49**, 867-872
9. Sun, H. B., Zhao, L., Tanaka, S., and Yokota, H. (2012) Moderate joint loading reduces degenerative actions of matrix metalloproteinases in the articular cartilage of mouse ulnae. *Connect Tissue Res* **53**, 180-186
10. Shim, J. W., Dodge, T. R., Hammond, M. A., Wallace, J. M., Zhou, F. C., and Yokota, H. (2014) Physical weight loading induces expression of tryptophan hydroxylase 2 in the brain stem. *PLoS One* **9**, e85095
11. Yang, S., Liu, H., Zhu, L., Li, X., Liu, D., Song, X., Yokota, H., and Zhang, P. (2019) Ankle loading ameliorates bone loss from breast cancer-associated bone metastasis. *FASEB J* **33**, 10742-10752.
12. Wang, L., Wang, Y., Chen, A., Teli, M., Kondo, R., Jalali, A., Fan, Y., Liu, S., Zhao, X., Siegel, A., Minami, K., Agarwal, M., Li, B. Y., and Yokota, H. (2019) Pitavastatin slows tumor progression and alters urine-derived volatile organic compounds through the mevalonate pathway. *FASEB J* **33**, 13710-13721)
13. da Silva PM. (2011) Are all statins the same? Focus on the efficacy and tolerability of pitavastatin. *Am J Cardiovasc Drugs* **11(2)**:93–107.
14. Wu D, Fan Y, Liu S, Woollam MD, Sun X, Murao E, Zha R, Prakash R, Park C, Siegel AP, Liu J, Agarwal M, Li BY, and Yokota H. (2020) Loading-induced anti-tumor capability of murine and human urine. *FASEB J* (in press)
15. Kopecka, J., Trouillas, P., Gasparovic, A. C., Gazzano, E., Assaraf, Y. G., and Riganti, C. (2020) Phospholipids and cholesterol: Inducers of cancer multidrug resistance and therapeutic targets. *Drug Resist Updat* **49**, 100670
16. Coughlin, T. R., Romero-Moreno, R., Mason, D. E., Nystrom, L., Boerckel, J. D., Niebur, G., and Littlepage, L. E. (2017) Bone: A Fertile Soil for Cancer Metastasis. *Curr Drug Targets* **18**, 1281-1295
17. Bikle, D. D. (2014) The vitamin D receptor: a tumor suppressor in skin. *Adv Exp Med Biol* **810**, 282-302
18. Prabhu, A. V., Luu, W., Li, D., Sharpe, L. J., and Brown, A. J. (2016) DHCR7: A vital enzyme switch between cholesterol and vitamin D production. *Prog Lipid Res* **64**, 138-151

19. Deng, W., Fernandez, A., McLaughlin, S. L., and Klinke, D. J., 2nd. (2019) WNT1-inducible signaling pathway protein 1 (WISP1/CCN4) stimulates melanoma invasion and metastasis by promoting the epithelial-mesenchymal transition. *J Biol Chem* **294**, 5261-5280
20. Al-Hendy, A., Diamond, M. P., Boyer, T. G., and Halder, S. K. (2016) Vitamin D3 Inhibits Wnt/beta-Catenin and mTOR Signaling Pathways in Human Uterine Fibroid Cells. *J Clin Endocrinol Metab* **101**, 1542-1551
21. Venkatesan, B., Prabhu, S. D., Venkatachalam, K., Mummidi, S., Valente, A. J., Clark, R. A., Delafontaine, P., and Chandrasekar, B. (2010) WNT1-inducible signaling pathway protein-1 activates diverse cell survival pathways and blocks doxorubicin-induced cardiomyocyte death. *Cell Signal* **22**, 809-820
22. Ewens, A., Mihich, E., and Ehrke, M. J. (2005) Distant metastasis from subcutaneously grown E0771 medullary breast adenocarcinoma. *Anticancer Res* **25**, 3905-3915
23. Liu, S., Fan, Y., Chen, A., Jalali, A., Minami, K., Ogawa, K., Nakshatri, H., Li, B. Y., and Yokota, H. (2018) Osteocyte-Driven Downregulation of Snail Restrains Effects of Drd2 Inhibitors on Mammary Tumor Cells. *Cancer Res* **78**, 3865-3876
24. Xu, W., Wan, Q., Na, S., Yokota, H., Yan, J. L., and Hamamura, K. (2015) Suppressed invasive and migratory behaviors of SW1353 chondrosarcoma cells through the regulation of Src, Rac1 GTPase, and MMP13. *Cell Signal* **27**, 2332-2342
25. Minami, K., Liu, S., Liu, Y., Chen, A., Wan, Q., Na, S., Li, B. Y., Matsuura, N., Koizumi, M., Yin, Y., Gan, L., Xu, A., Li, J., Nakshatri, H., and Yokota, H. (2017) Inhibitory Effects of Dopamine Receptor D1 Agonist on Mammary Tumor and Bone Metastasis. *Sci Rep* **7**, 45686
26. Woollam, M., Teli, M., Angarita-Rivera, P., Liu, S., Siegel, A. P., Yokota, H., and Agarwal, M. (2019) Detection of Volatile Organic Compounds (VOCs) in Urine via Gas Chromatography-Mass Spectrometry QTOF to Differentiate Between Localized and Metastatic Models of Breast Cancer. *Sci Rep* **9**, 2526
27. Tang, Z., Li, C., Kang, B., Gao, G., Li, C., and Zhang, Z. (2017) GEPIA: a web server for cancer and normal gene expression profiling and interactive analyses. *Nucleic Acids Res* **45**, W98-W102
28. Ferrari, N., McDonald, L., Morris, J. S., Cameron, E. R., and Blyth, K. (2013) RUNX2 in mammary gland development and breast cancer. *J Cell Physiol* **228**, 1137-1142
29. Yousef, E. M., Tahir, M. R., St-Pierre, Y., and Gaboury, L. A. (2014) MMP-9 expression varies according to molecular subtypes of breast cancer. *BMC Cancer* **14**, 609
30. De Craene, B., and Berx, G. (2006) Snail in the frame of malignant tumor recurrence. *Breast Cancer Res* **8**, 105
31. Pauli, C., Hopkins, B. D., Prandi, D., Shaw, R., Fedrizzi, T., Sboner, A., Sailer, V., Augello, M., Puca, L., Rosati, R., McNary, T. J., Churakova, Y., Cheung, C., Triscott, J., Pisapia, D., Rao, R., Mosquera, J. M., Robinson, B., Faltas, B. M., Emerling, B. E., Gadi, V. K., Bernard, B., Elemento, O., Beltran, H., Demichelis, F., Kemp, C. J., Grandori, C., Cantley, L. C., and Rubin, M. A. (2017) Personalized In Vitro and In Vivo Cancer Models to Guide Precision Medicine. *Cancer Discov* **7**, 462-477
32. Wang, T. J., Chang, C. F., Lou, M. F., Ao, M. K., Liu, C. C., Liang, S. Y., Wu, S. F., and Tung, H. H. (2015) Biofeedback relaxation for pain associated with continuous passive motion in Taiwanese patients after total knee arthroplasty. *Res Nurs Health* **38**, 39-50
33. Holm, N. J., Moller, T., Adamsen, L., Dalsgaard, L. T., Biering-Sorensen, F., and Schou, L. H. (2019) Health promotion and cardiovascular risk reduction in people with spinal cord injury: physical activity, healthy diet and maintenance after discharge- protocol for a prospective national cohort study and a preintervention- postintervention study. *BMJ Open* **9**, e030310
34. Guo, S., Huang, Y., Zhang, Y., Huang, H., Hong, S., and Liu, T. (2020) Impacts of exercise interventions on different diseases and organ functions in mice. *J Sport Health Sci* **9**, 53-73

Figure Legends

Figure 1

Reduction in bone loss by knee loading. The single and double asterisks indicate $p < 0.05$ and $p < 0.01$, respectively. (A) Schematic illustration of intra-tibia injection of EO771 mammary tumor cells and the timeline. (B) Representative μCT images of the proximal tibia. (C) Comparison of BV/TV, BMD, Tb.n, and Tb.s in the proximal tibia between the placebo and loaded groups. (D) Representative μCT images of the distal femur. (E) Comparison of BV/TV, BMD, Tb.n, and Tb.s in the distal femur between the placebo and loaded groups. (F) HE staining of the proximal tibia in the placebo and loaded groups, and the relative tumor area. The dotted area (green) indicates the tumor-grown region. (G) Reduction in the protein levels of MMP9, Runx2, TGFβ, and Snail in bone marrow-derived cells in the loaded group.

Figure 2

Load-driven reduction in the mammary tumor. The single and double asterisks indicate $p < 0.05$ and $p < 0.01$, respectively. (A) Schematic illustration of the injection of EO771 mammary tumor cells to the mammary fat pad. (B) Mammary tumors 2 weeks after tumor inoculation in the placebo and loaded group. (C&D) Decrease in the tumor weight and size in the loaded group.

Figure 3

Load-driven alterations in urinary volatile organic compounds (VOCs). Of note, PCA = principal component axis. The single and double asterisks indicate $p < 0.05$ and $p < 0.01$, respectively. (A) Hierarchical clustergram for the normal, placebo, and loaded groups, including 22 VOCs. (B&C) Principal component plots for the urine samples and 22 VOCs, respectively. (D) Mevalonate pathway leading to cholesterol synthesis including 5 VOCs (alpha/beta-farnesene, linalool, isoprenul alcohol, and beta-pinene) that were enriched in the placebo group.

Figure 4

Effects of TGFβ and calcitriol in the urine. Of note, CN = control, pl = placebo, load = knee loading, and VD = vitamin D3 (calcitriol). The single and double asterisks indicate $p < 0.05$ and $p < 0.01$, respectively. (A) Cholesterol levels in the serum and urine in the normal, placebo, and loaded groups. (B) TGFβ levels in the serum and urine before and after knee loading. (C) Effects of TGFβ on the expression of MMP9, Runx2, and Snail. (D) Calcitriol levels in the serum and urine before and after knee loading. (E) Effects of calcitriol on the expression of MMP9, Runx2, and Snail. (F-H) Calcitriol-driven reduction in EdU-based proliferation, Transwell invasion, and cellular motility of EO771 cells.

Figure 5

Load-driven downregulation of WISP1 in the post-loading murine urine. Of note, CN = control, and VD = vitamin D3 (calcitriol). (A) Expression of 111 cytokines and chemokines in the mouse XL cytokine array. (B-D) WISP1-driven stimulation of EdU-based proliferation, Transwell invasion, and cellular motility of EO771 cells. (E) Elevation of MMP9, Runx2, TGFβ, and Snail by WISP1 in EO771 cells. (F) Size changes in fragmented breast cancer tumor tissue by calcitriol and WISP1.

Figure 6

Differential effects of pre- and post-loading urine samples on the expression of WISP1, MMP9, Runx2, and TGFβ in EO771 cells. Of note, pre-S & post-S = pre- & post-step aerobics, and pre-L & post-L = pre- and post-loading. The bar chart is based on 10 pairs of human samples and 10 pairs of mouse samples. (A&B) Downregulation of MMP9, RUNX2, TGFβ, and WISP1 in response to human post-step aerobics urine samples. (C&D) Downregulation of MMP9, RUNX2, TGFβ, and WISP1 in response to murine post-knee loading urine samples.

Figure 7

WISP1 expression in TCGA and GTEx databases. (A) Elevated level of WISP1 transcripts in patients with breast cancer. (B) Significant reduction in the overall survival rate for patients with a high level of WISP1. (C) Correlation of transcript levels among WISP1, TGFβ, Runx2, and Snail in skeletal tissues. (D) Correlation of transcript levels among WISP1, TGFβ, Runx2, and MMP9 in breast cancer tissues. (E) Proposed mechanism for load-driven suppression of tumor progression, in which knee loading upregulated vitamin D3 (calcitriol) and downregulated cholesterol and TGFβ, which downregulated WISP1, MMP9, and Snail.

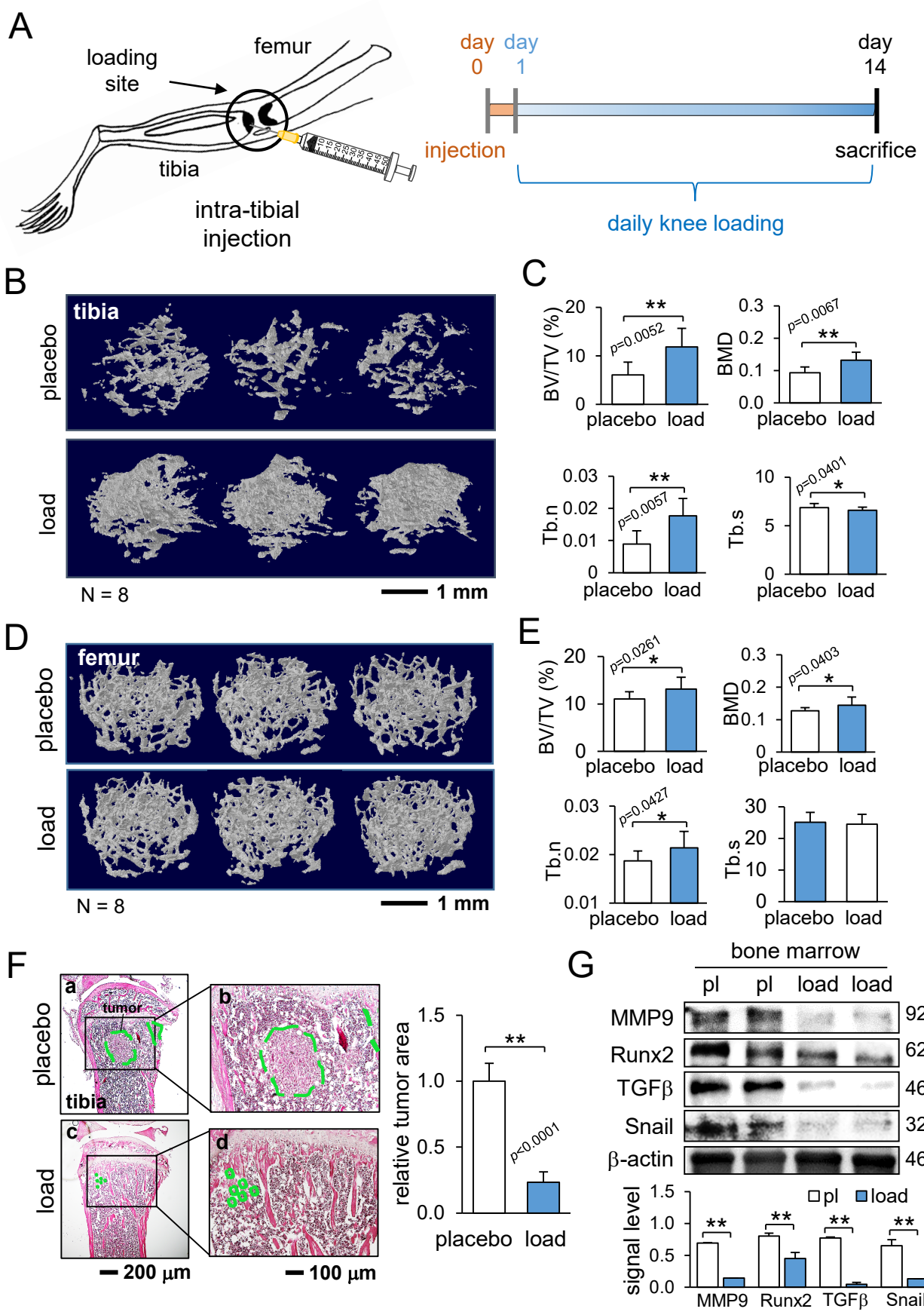
A
loading site
femur
tibia
intra-tibial injection
day 0
day 1
day 14
injection
sacrifice
daily knee loading
B
tibia
placebo
load
N = 8
1 mm
C
BV/TV (%)
p=0.0052
BMD
p=0.0067
Tb.n
p=0.0057
Tb.s
p=0.0401
placebo
load
D
femur
placebo
load
N = 8
1 mm
E
BV/TV (%)
p=0.0261
BMD
p=0.0403
Tb.n
p=0.0427
Tb.s
placebo
load
F
a
tumor
tibia
b
c
d
placebo
load
200 μm
100 μm
relative tumor area
p<0.0001
placebo
load
G
bone marrow
pl
pl
load
load
MMP9
Runx2
TGFβ
Snail
β-actin
92kDa
62kDa
46kDa
32kDa
46kDa
signal level
pl
load
MMP9
Runx2
TGFβ
Snail

Figure 1

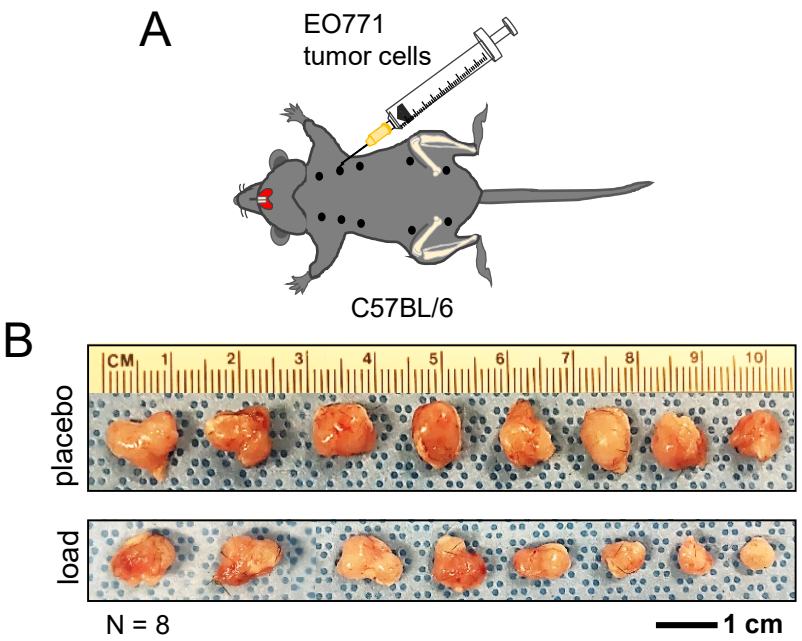
A
EO771
tumor cells
C57BL/6
B
CM 1 2 3 4 5 6 7 8 9 10
placebo
load
N = 8
1 cm
C
tumor weight (g)
0.3
0.2
0.1
0.0
p=0.0267
*
placebo
load
D
tumor size (cm3)
1.5
1.0
0.5
0.0
p=0.0006
**
placebo
load

Figure 2

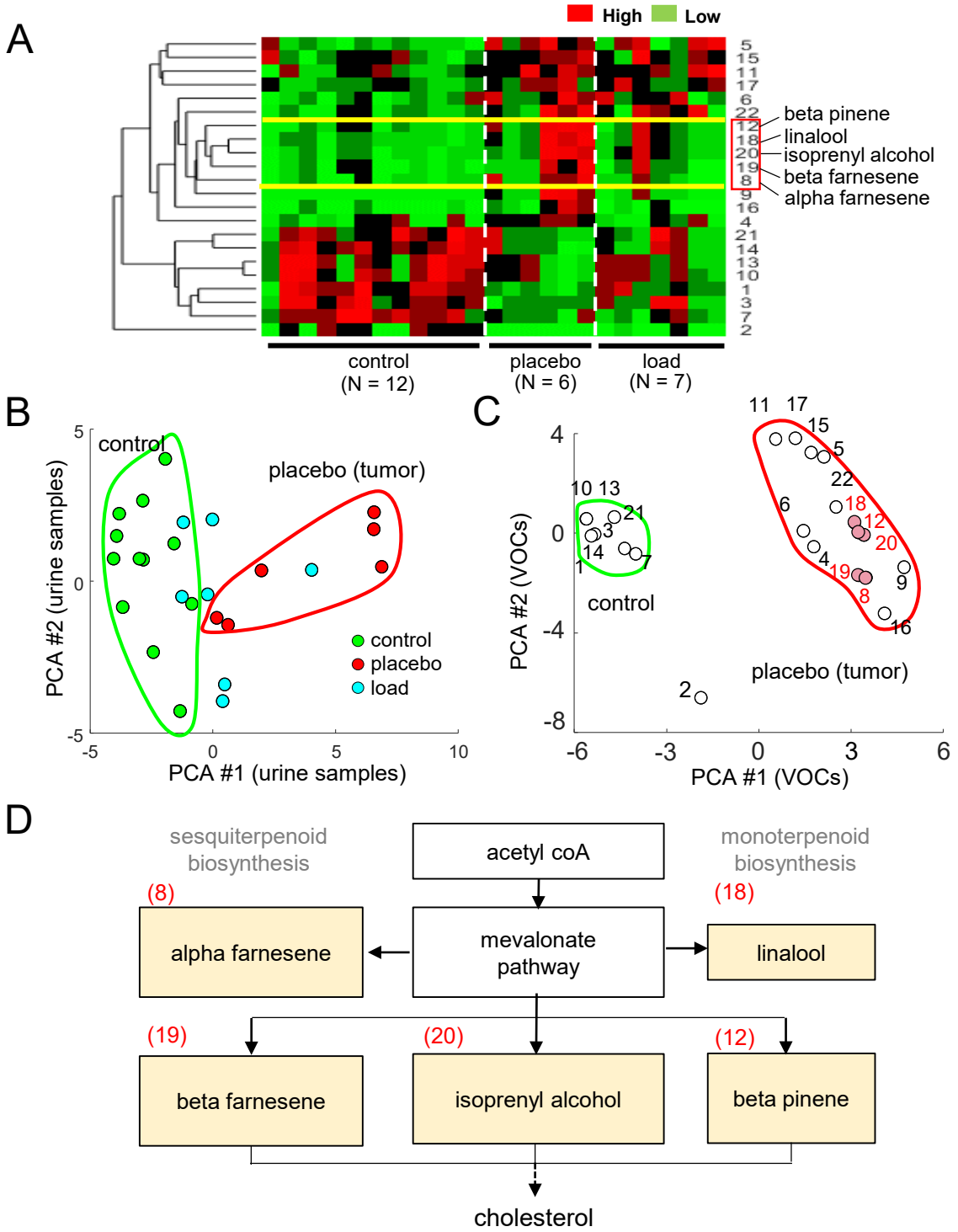
A
High
Low
beta pinene
linalool
isoprenyl alcohol
beta farnesene
alpha farnesene
control
(N = 12)
placebo
(N = 6)
load
(N = 7)
B
control
placebo (tumor)
control
placebo
load
PCA #2 (urine samples)
PCA #1 (urine samples)
C
control
placebo (tumor)
PCA #2 (VOCs)
PCA #1 (VOCs)
D
sesquiterpenoid biosynthesis
acetyl coA
monoterpenoid biosynthesis
(8)
(18)
alpha farnesene
mevalonate pathway
linalool
(19)
(20)
(12)
beta farnesene
isoprenyl alcohol
beta pinene
cholesterol

Figure 3

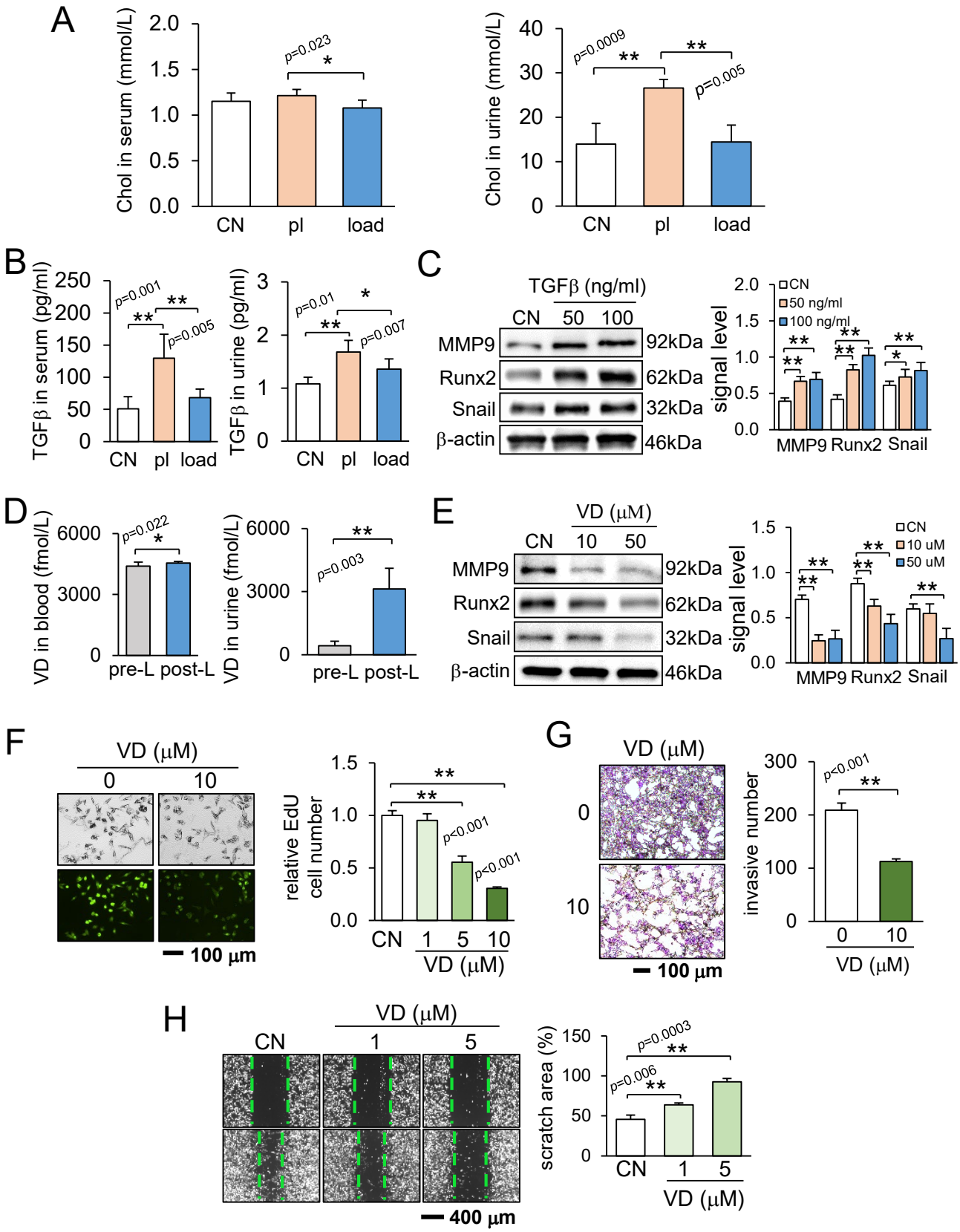
A
Chol in serum (mmol/L)
2.0
1.5
1.0
0.5
0.0
p=0.023
*
CN
pl
load
Chol in urine (mmol/L)
40
30
20
10
0
p=0.0009
**
**
p=0.005
CN
pl
load
B
TGFβ in serum (pg/ml)
250
200
150
100
50
0
p=0.001
**
**
p=0.005
CN
pl
load
TGFβ in urine (pg/ml)
3
2
1
0
p=0.01
**
*
p=0.007
CN
pl
load
C
TGFβ (ng/ml)
CN
50
100
MMP9
Runx2
Snail
β-actin
92kDa
62kDa
32kDa
46kDa
signal level
2.0
1.5
1.0
0.5
0.0
CN
50 ng/ml
100 ng/ml
MMP9
Runx2
Snail
D
VD in blood (fmol/L)
6000
3000
0
p=0.022
*
pre-L
post-L
VD in urine (fmol/L)
6000
3000
0
**
p=0.003
pre-L
post-L
E
VD (μM)
CN
10
50
MMP9
Runx2
Snail
β-actin
92kDa
62kDa
32kDa
46kDa
signal level
1.5
1.0
0.5
0.0
CN
10 uM
50 uM
MMP9
Runx2
Snail
F
VD (μM)
0
10
100 μm
relative EdU cell number
1.5
1.0
0.5
0.0
**
**
p<0.001
p<0.001
CN
1
5
10
VD (μM)
G
VD (μM)
0
10
100 μm
invasive number
300
200
100
0
p<0.001
**
0
10
VD (μM)
H
VD (μM)
CN
1
5
400 μm
scratch area (%)
150
100
50
0
p=0.0003
**
p=0.006
**
CN
1
5
VD (μM)

Figure 4

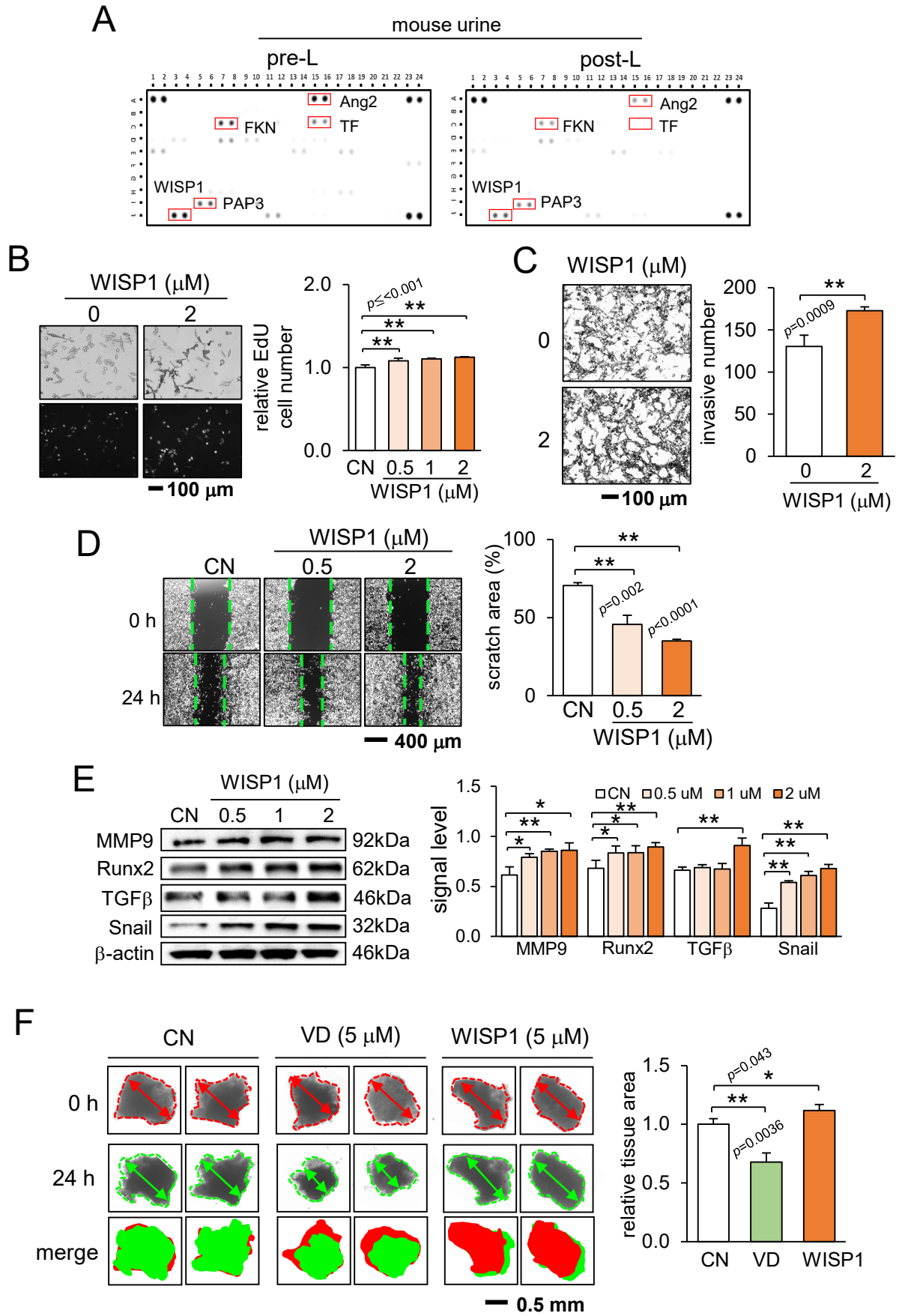
A
mouse urine
pre-L
post-L
Ang2
TF
FKN
WISP1
PAP3
B
WISP1 (μM)
0
2
100 μm
relative EdU cell number
p≤<0.001
CN 0.5 1 2
WISP1 (μM)
C
WISP1 (μM)
invasive number
p=0.0009
0 2
WISP1 (μM)
100 μm
D
WISP1 (μM)
CN 0.5 2
0 h
24 h
400 μm
scratch area (%)
p=0.002
p<0.0001
CN 0.5 2
WISP1 (μM)
E
WISP1 (μM)
CN 0.5 1 2
MMP9 92kDa
Runx2 62kDa
TGFβ 46kDa
Snail 32kDa
β-actin 46kDa
CN 0.5 uM 1 uM 2 uM
signal level
MMP9 Runx2 TGFβ Snail
F
CN
VD (5 μM)
WISP1 (5 μM)
0 h
24 h
merge
0.5 mm
relative tissue area
p=0.043
p=0.0036
CN VD WISP1

Figure 5

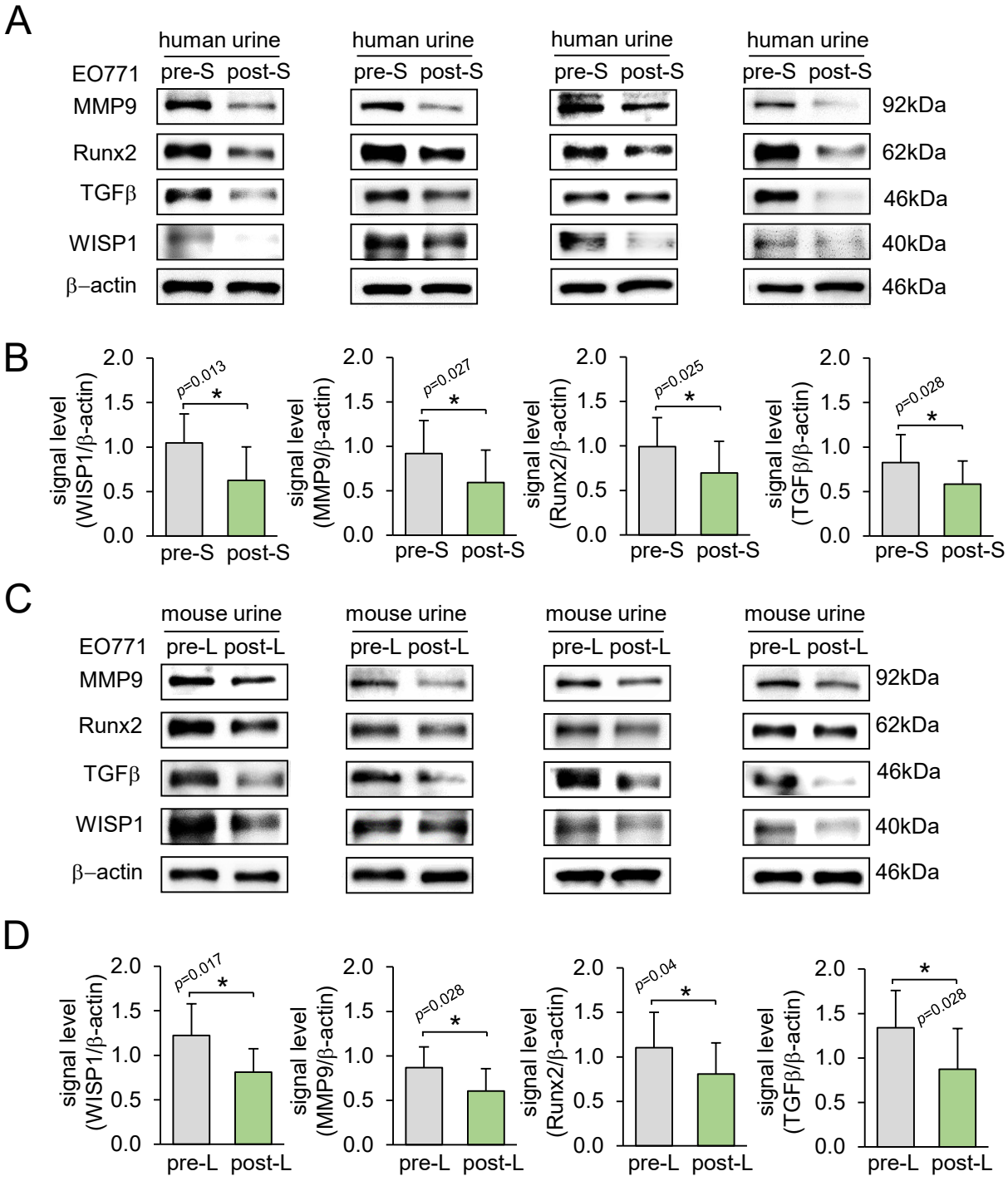
A
human urine
EO771
pre-S post-S
MMP9
Runx2
TGFβ
WISP1
β–actin
92kDa
62kDa
46kDa
40kDa
46kDa
B
signal level (WISP1/β-actin)
signal level (MMP9/β-actin)
signal level (Runx2/β-actin)
signal level (TGFβ/β-actin)
p=0.013
p=0.027
p=0.025
p=0.028
pre-S post-S
C
mouse urine
pre-L post-L
D
p=0.017
p=0.028
p=0.04
p=0.028

Figure 6

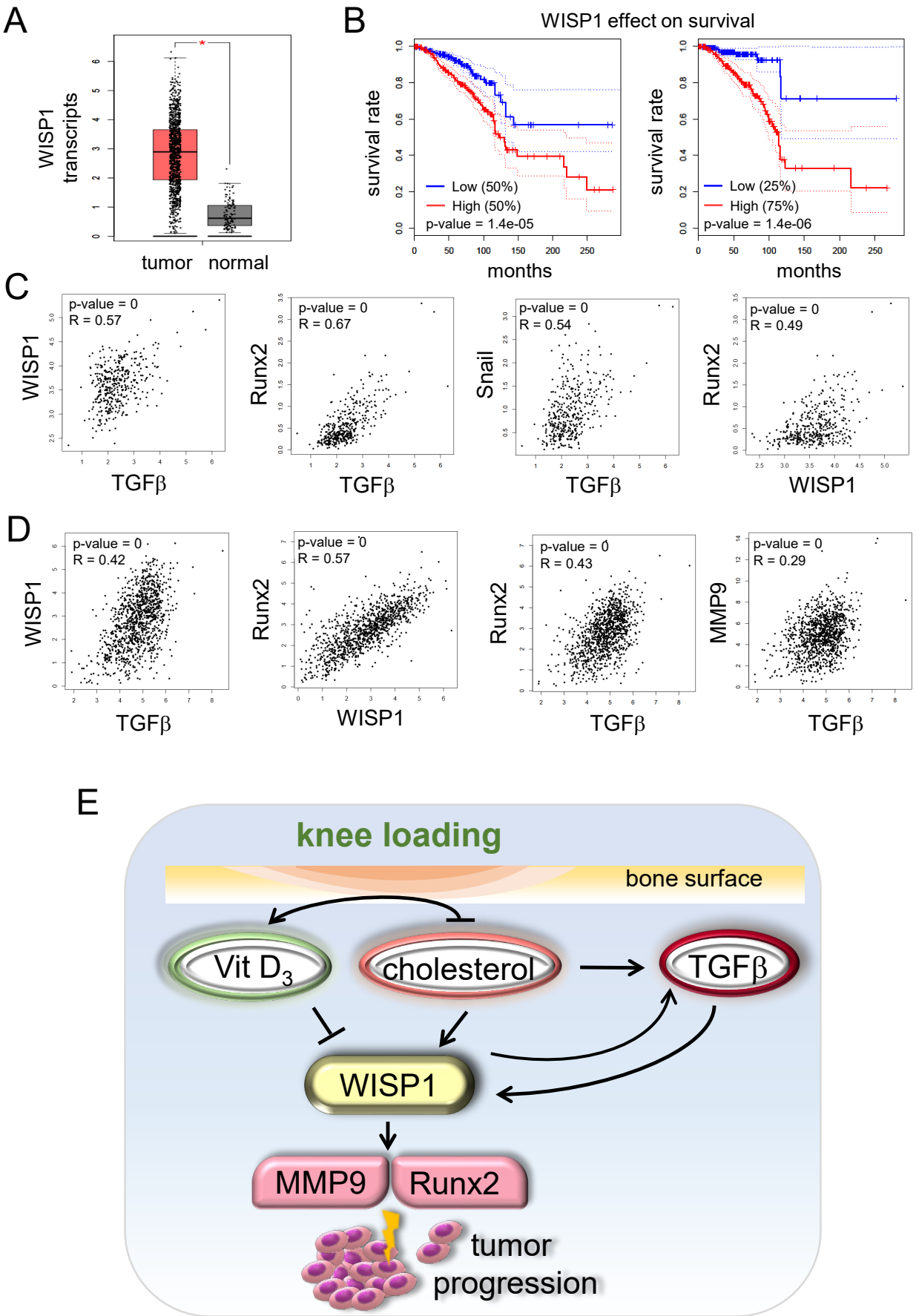
A
WISP1 transcripts
tumor
normal
B
WISP1 effect on survival
survival rate
Low (50%)
High (50%)
p-value = 1.4e-05
months
Low (25%)
High (75%)
p-value = 1.4e-06
C
WISP1
TGFβ
p-value = 0
R = 0.57
Runx2
p-value = 0
R = 0.67
Snail
p-value = 0
R = 0.54
Runx2
p-value = 0
R = 0.49
D
WISP1
TGFβ
p-value = 0
R = 0.42
Runx2
WISP1
p-value = 0
R = 0.57
Runx2
TGFβ
p-value = 0
R = 0.43
MMP9
TGFβ
p-value = 0
R = 0.29
E
knee loading
bone surface
Vit D3
cholesterol
TGFβ
WISP1
MMP9
Runx2
tumor
progression

Figure 7

Supplementary Information

Loading-driven WISP1 downregulation for tumor suppression with a urinary balance shift from cholesterol to calcitriol

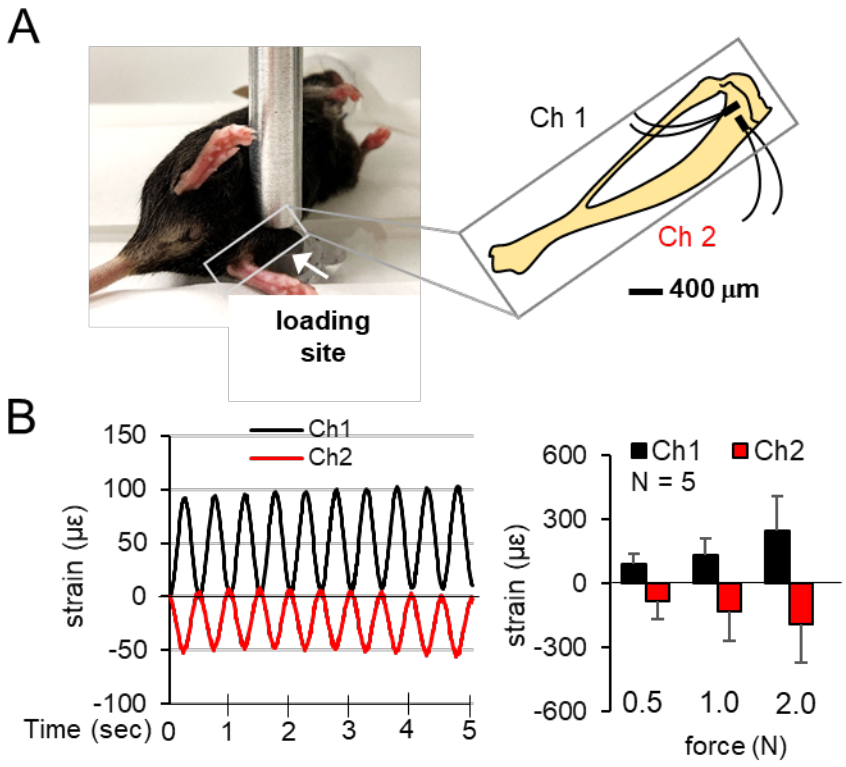

Suppl. Figure S1. Knee loading and strain measurements. (A) Setup for knee loading. (B) Strain on the proximal tibia in response to 0.5 to 2 N sinusoidal loading at 2 Hz.

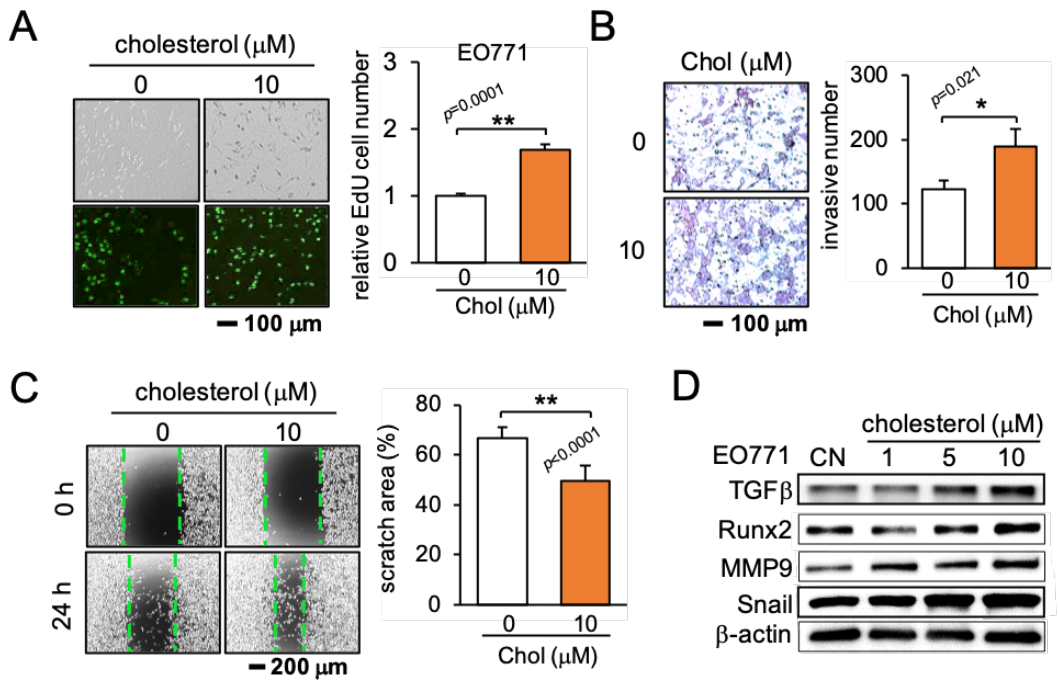

Suppl. Figure S2. Effects of cholesterol in proliferation, invasion and migration of EO771 cells. The single and double asterisks indicate $p < 0.05$ and $p < 0.01$, respectively. (A) Increase in EdU-based cellular proliferation by cholesterol. (B&C) Elevated invasion and migration by cholesterol, respectively. (D) Cholesterol-driven increase in the protein levels of TGFβ, Runx2, MMP9, and Snail.

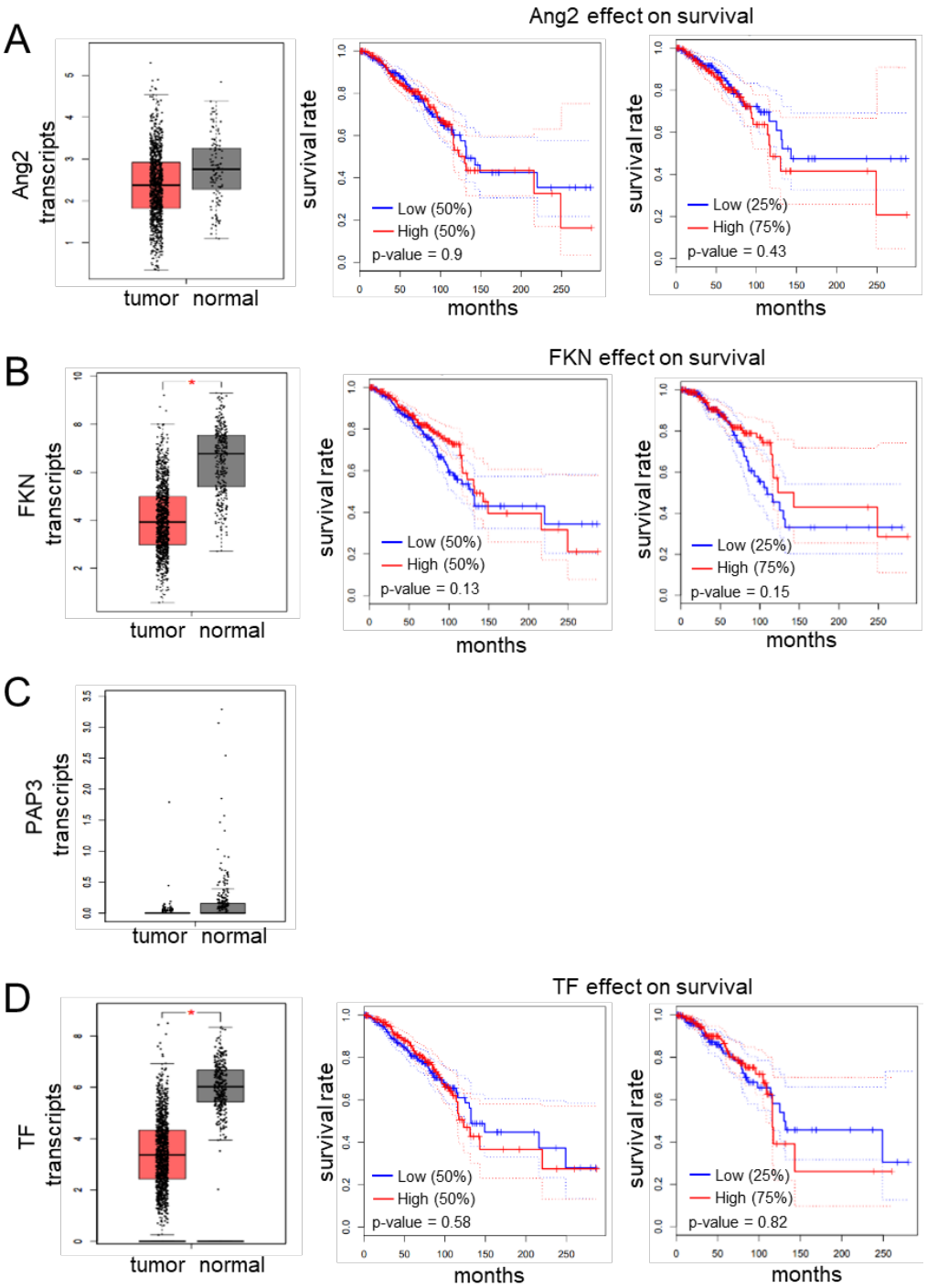

Suppl. Figure S3. Transcript levels and an overall survival rate in TCGA and GTEx databases for 4 genes, which were identified as a potential loading-driven regulatory target in the protein array analysis. Of note, Ang2 = angiopoietin 2, FKN = fractalkine, PAP3 = purple acid phosphatase 3, and TF = transferrin. (A) Ang2 transcript level and the overall survival rate. (B) FKN transcript level and the overall survival rate. (C) PAP3 transcript level. The overall survival rate was not available because of the insufficient sample size. (D) TF transcript level and the overall survival rate.

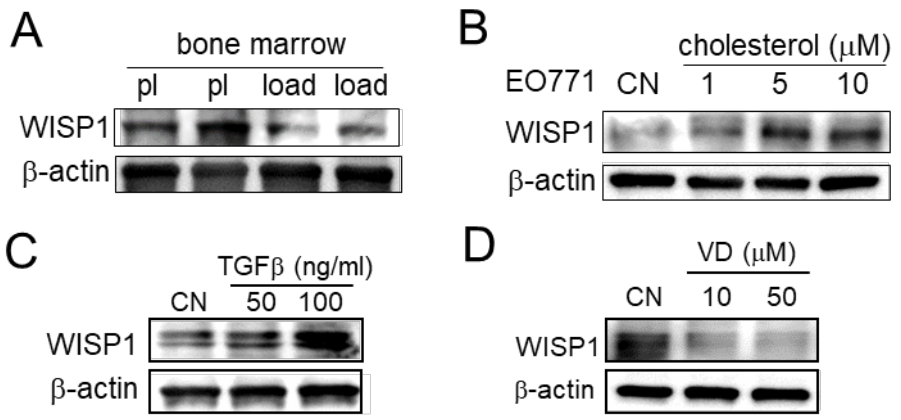

Suppl. Figure S4. WISP1 expression. Of note, pl = placebo, load = knee loading, and CN = control. (A) WISP1 expression in tibial bone marrow-derived cells in the placebo and loaded groups. (B) WISP1 expression in EO771 mammary tumor cells in response to cholesterol. (C&D) WISP1 expression in EO771 mammary tumor cells in response to TGFβ and vitamin D_3 (calcitriol), respectively.

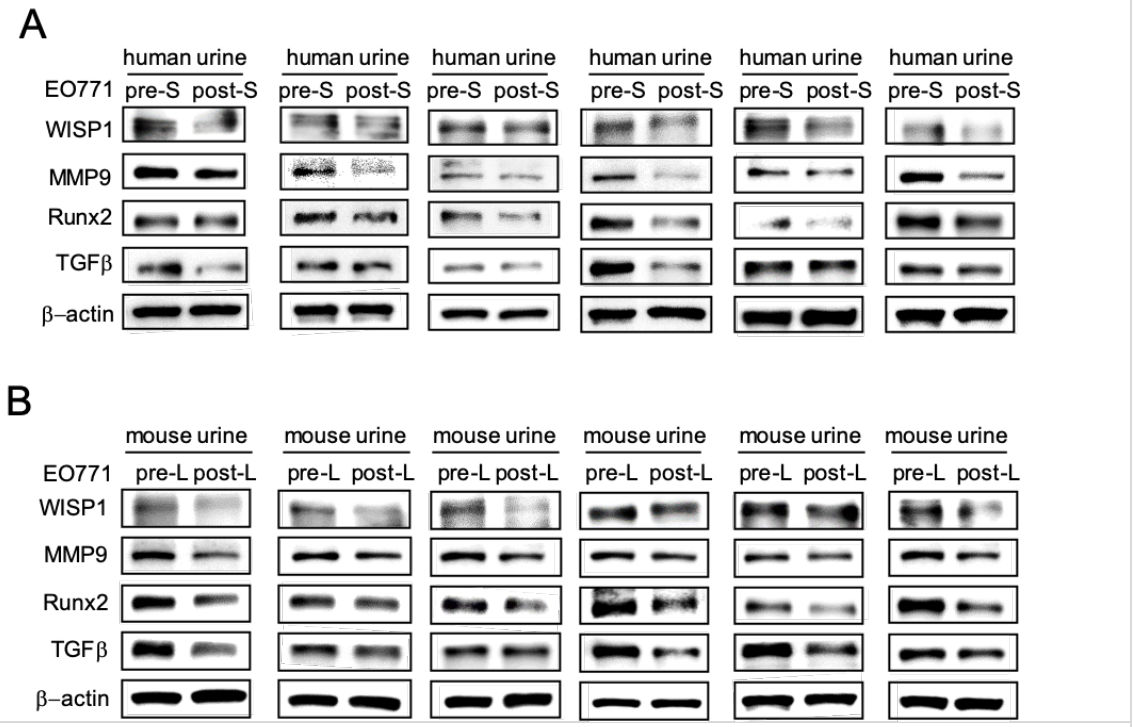

Suppl. Figure S5. Expression of WISP1, MMP9, Runx2, and TGFβ in EO771 cells in response to urine (2% in culture medium) before and after mechanical stimulation. Of note, pre-S & post-S = pre- & post-step aerobics, and pre-L & post-L = pre- and post-loading. (A) Responses to 6 pairs of human urine samples before and after 10-min step aerobics. (B) Responses to 6 pairs of murine urine samples before and after 5-min knee loading.